

Parameterization-driven Neural Implicit Surfaces Editing

Baixin Xu¹, Jiangbei Hu^{1,2}, Fei Hou³, Kwan-Yee Lin^{4,5}, Wayne Wu⁵, Chen Qian⁶, Ying He¹

¹ Nanyang Technological University ² Dalian University of Technology

³ Institute of Software, Chinese Academy of Sciences ⁴ The Chinese University of Hong Kong

⁵ Shanghai AI Laboratory ⁶ SenseTime Research

yhe@ntu.edu.sg

Abstract

The growing capabilities of neural rendering have increased the demand for new techniques that enable intuitive editing of 3D objects, particularly when they are represented as neural implicit surfaces. In this paper, we present a novel neural algorithm to parameterize neural implicit surfaces to simple parametric domains, such as spheres, cubes, or polycubes, thereby facilitating visualization and various editing tasks. Technically, our method computes a bi-directional deformation between 3D objects and their chosen parametric domains, eliminating the need for any prior information. We adopt a forward mapping of points on the zero level set of the 3D object to a parametric domain, followed by a backward mapping through inverse deformation. To ensure the map is bijective, we employ a cycle loss while optimizing the smoothness of both deformations. Additionally, we leverage a Laplacian regularizer to effectively control angle distortion and offer the flexibility to choose from a range of parametric domains for managing area distortion. Designed for compatibility, our framework integrates seamlessly with existing neural rendering pipelines, taking multi-view images as input to reconstruct 3D geometry and compute the corresponding texture map. We also introduce a simple yet effective technique for intrinsic radiance decomposition, facilitating both view-independent material editing and view-dependent shading editing. Our method allows for the immediate rendering of edited textures through volume rendering, without the need for network re-training. Moreover, our approach supports the co-parameterization of multiple objects and enables texture transfer between them. We demonstrate the effectiveness of our method on images of human heads and man-made objects. We will make the source code publicly available.

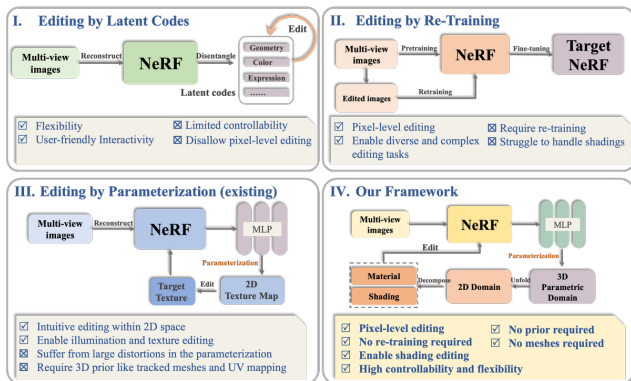


Figure 1. Overview of NeRF-based editing work. We summarize the existing work into three main categories: manipulating the latent codes, re-training, and parameterization. In this study, we propose a novel NeRF editing method based on our 3D neural parameterization framework.

1. Introduction

Neural radiance fields (NeRF) [29] have garnered remarkable success in both the computer vision and computer graphics communities, redefining benchmarks for high-quality renderings and novel view synthesis. Building upon NeRF, a variety of methods leveraging implicit neural representations [32, 47, 61] have emerged, delivering high-fidelity 3D reconstructions. The demand for intuitive 3D object editing techniques has increased with the growing capabilities of neural rendering, especially for neural implicit surfaces. Extensive explorations have been made in editing within the Neural Rendering framework to achieve diverse visual effects. By manipulating the latent codes of the network, one can implicitly alter the shape and color of 3D objects [25, 54, 63]. In the work of [20, 45], palette-based methods have been employed to facilitate transformations in the color and style of rendered scenes. However, these methods suffer from limited controllability and disallow local pixel editing. Seal3D [48] proposed a teacher-student

training strategy to edit the interactive scene at the pixel level. Yet, this method is tricky to handle shading, and each subsequent edit required a new training iteration. By employing neural networks to formulate a differentiable surface parameterization, it can be facilitated to edit textures or shapes within the neural rendering pipeline [27, 53]. Existing neural parameterization techniques still face significant challenges, such as the need for appropriate distortion constraints to ensure accurate detail reconstruction or reducing the reliance on prior information from tracked mesh and UV mapping. The final quality of edited visual effects is significantly impacted by these issues. We summarize the main work related to NeRF-editing in Fig. 1.

This paper aims at developing an intuitive and easy-to-use tool for appearance editing in neural implicit surfaces. Towards this goal, we propose a novel method to parameterize neural implicit surfaces to parametric domains where the radiance field is represented as a texture map. Distinguished from previous work that using 2D texture mapping, our neural parameterization algorithm supports the selection of different 3D parametric domains according to geometric shapes to avoid seams and reduce distortion, such as spheres, cubes, and polycubes. Technically, our parameterization algorithm utilizes a neural network to learn a bi-directional deformation between 3D objects and the chosen parametric domains. This involves a forward deformation that maps points from the zero level set of the neural implicit surface to the parametric domain, followed by an inverse deformation, mapping points backward. Notably, we do not require any explicit prior information in learning both deformations. We employ a cycle loss to ensure the smoothness of the bi-directional deformation, and a Laplacian regularization to effectively control angle distortion. Our method also supports the flexible selection of parametric domains for controlling area distortion. With the parametrization, 3D radiance field is mapped to a simple 3D parametric domain which can be further disassembled into a 2D domain, facilitating visualization and various editing tasks. Furthermore, we decompose the 2D radiance field into two components: view-independent material and view-dependent shading, streamlining both texture and shading editing. Our neural parameterization algorithm is fully compatible with existing neural rendering pipelines, allowing 3D reconstruction from multi-view images as input and the creation of texture maps simultaneously. It allows for the immediate rendering of edited textures through volume rendering, without network re-training. Moreover, it supports co-parameterization of objects of similar geometry and enables texture transfer between them. We validate the effectiveness of our method on scenes of human heads and man-made objects. Our contributions are summarized as follows:

- We present a neural parameterization framework that

computes bi-directional deformation between 3D objects and their parametric domains, eliminating the need for any prior information from tracked mesh or UV mapping. Our approach utilizes Laplacian loss to minimize angle distortion and provides a choice of 3D parametric domains, such as spheres, cubes, or polycubes, to control area distortion.

- We introduce a simple yet effective technique for intrinsic radiance decomposition, facilitating both view-independent texture editing and view-dependent shading editing.
- Our neural parameterization framework is fully compatible with existing neural rendering architectures, accepting multi-view images as input to reconstruct 3D geometry and generate UV maps as output. Additionally, it enables the direct rendering of modified textures using the volume rendering pipeline.
- Our approach supports co-parameterization of multiple objects and allows for texture transfer between different objects.

2. Related Work

Parameterization. Surface parameterization [6, 41] aims at computing a bijective mapping between the 3D surface and a suitable parametric domain, usually a 2D region or a simple 3D object, such as spheres [9] and polycubes [8, 44]. Serving as an important computational tool in computer graphics and digital geometry processing [41], surface parameterization facilitates various applications, including texture editing [5], surface painting [43], details transfer [2], remeshing [35], among others. Neural networks are now commonly used in digital geometry processing, resulting in the creation of parameterization algorithms based on deep learning techniques [1, 11, 14, 51]. Unlike classical methods that yield global and seamless parametrization, most neural parameterization methods are computing local parametrization [11, 66, 67]. These methods typically partition the 3D model into multiple patches and parameterize each to a 2D region, possibly followed by a post-processing step to stitch the patches together. Although these methods are efficient and can handle surfaces of arbitrary geometry and topology, they frequently encounter problems including non-bijectivity, a lack of smoothness, the presence of seams and overlaps, and large distortions. There are also works on neural parametric surfaces, defined in rectangular domains [26] and n -sided patches [59]. They can model complex surface geometries with high precision; however, such representations are not applicable to neural implicit surfaces and thereby incompatible with neural rendering.

Neural Implicit Functions. Recent years have seen a surge in the successful application of neural implicit functions within the realm of 3D deep learning. Compared to explicit representations such as point clouds [37], vox-

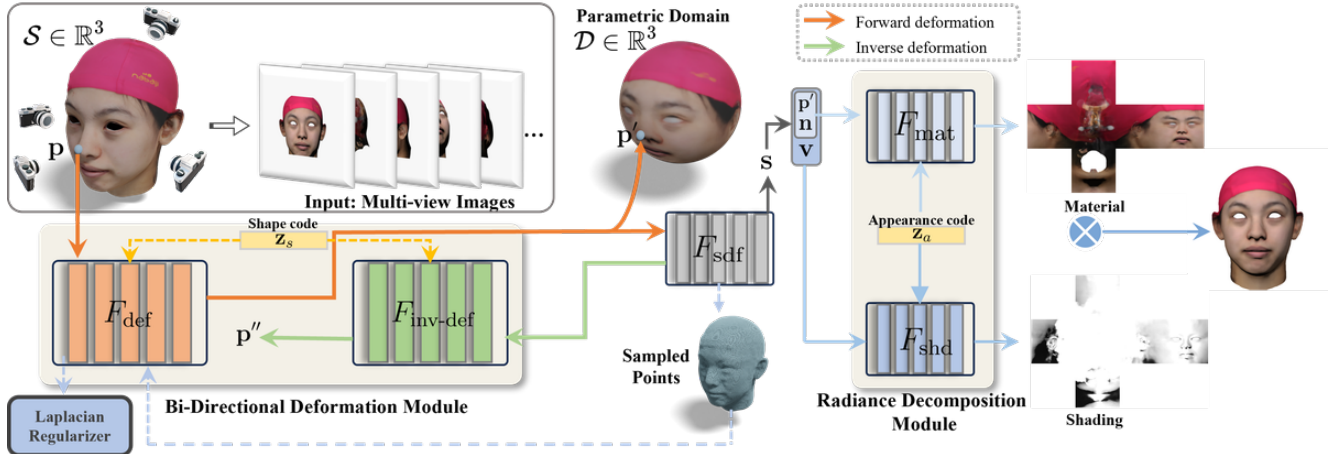


Figure 2. **Algorithmic pipeline.** Our network consists of three modules: bi-directional deformation (F_{def} and $F_{inv-def}$), geometry reconstruction (F_{sdf}) and radiance decomposition (F_{mat} and F_{shd}).

els [36], and meshes [46], neural implicit representations offer unique advantages including flexibility, continuity, and robustness [28, 33, 40]. When integrated within the neural rendering pipeline, neural implicit surfaces exhibit exceptional quality in 3D reconstructions from multi-view images [21, 22, 30, 38, 49, 50, 54]. However, as geometries and radiance fields are encoded as network parameters, editing them becomes complex and non-intuitive, compared to explicit representations. This paper aims at tackling this challenge by explicitly representing radiance fields as texture mapping that encompasses both view-dependent and view-independent components.

NeRF Editing. Numerous studies have focused on editing neural radiance fields, including relighting [23, 42], composition [34, 56], content generation [31], and shape editing [24, 65]. Editing tools operating at the scene- or object-level, such as [16, 56, 63], utilize latent codes to modify and stylize the appearance of an object or entire scenes. Conversely, pixel-level editing tools, such as NeuMesh [57] and Seal3D [48], utilize training-based approaches to edit fine-grained details. However, NeuMesh relies on explicit meshes which lack efficiency and robustness. Although Seal3D achieves interactive editing, it still suffers from poor geometry reconstruction and cannot change the illumination scene. Parameterization-based methods, such as NeuTex [53], ISO-UVField [39] and NeP [27], integrate the learning of UV mapping into the neural rendering framework, providing an intuitive means for editing within 2D domains. However, these methods often suffer from large distortions in the parametrization. Furthermore, they require 3D prior information from tracked meshes and UV mapping - conditions that may not be readily met in practical, real-world scenarios. IntrinsicNeRF [62] enhances standard neural radiance fields by gen-

erating additional outputs, including reflectance, shading, and a residual term. Incorporating a semantic branch, it facilitates real-time scene editing. However, it often results in aggregated colors, akin to palette-based methods [20, 45], hence cannot offer fine-grained editing results at the pixel level. Our approach decomposes the radiance field into view-dependent shadings and view-independent materials. Both components are represented as textures, enabling intuitive material modifications while preserving consistent shading.

3. Method

The input of our method is a collection of RGB images, denoted $\mathcal{I} = \{\mathbf{I}_i\}$, representing either multiple objects of similar geometry or a single object, captured from different viewpoints. To differentiate among objects, we assign a latent shape code \mathbf{z}_s and an appearance code \mathbf{z}_a to each object. This facilitates the co-parameterization of multiple objects and enables the transfer of material and shading among them. As illustrated in Figure 2, our method reconstructs 3D geometry as a neural implicit surface and encodes the 3D radiance field in a simple parametric domain, such as spheres and polycubes. For each input image, we randomly select a set of pixels. Then, for each pixel, we shoot a ray originating from the location of camera and traversing through the pixel. If the ray intersects with the surface, at a point, denoted as \mathbf{p} , we compute its corresponding position in the parametric domain \mathcal{D} , denoted as \mathbf{p}' , via a bi-directional deformation (Sec. 3.1): the forward deformation (depicted in orange) generates a displacement vector so that the updated position \mathbf{p}' is in the parametric domain; subsequently, the inverse deformation (depicted in green) maps \mathbf{p}' back to a point \mathbf{p}'' , which is anticipated to be in close proximity to the surface. We incorporate a cycle loss to penalize occur-

rences where \mathbf{p}'' deviates from \mathbf{p} . In addition, we employ a Laplacian loss (Sec. 3.2) to effectively reduce the angle distortion between the parametric domain and the original surface. Furthermore, we decompose the radiance into a view-independent material field and a view-dependent shading field (Sec. 3.3), each of which can be edited independently, thus augmenting the editing capability of our framework.

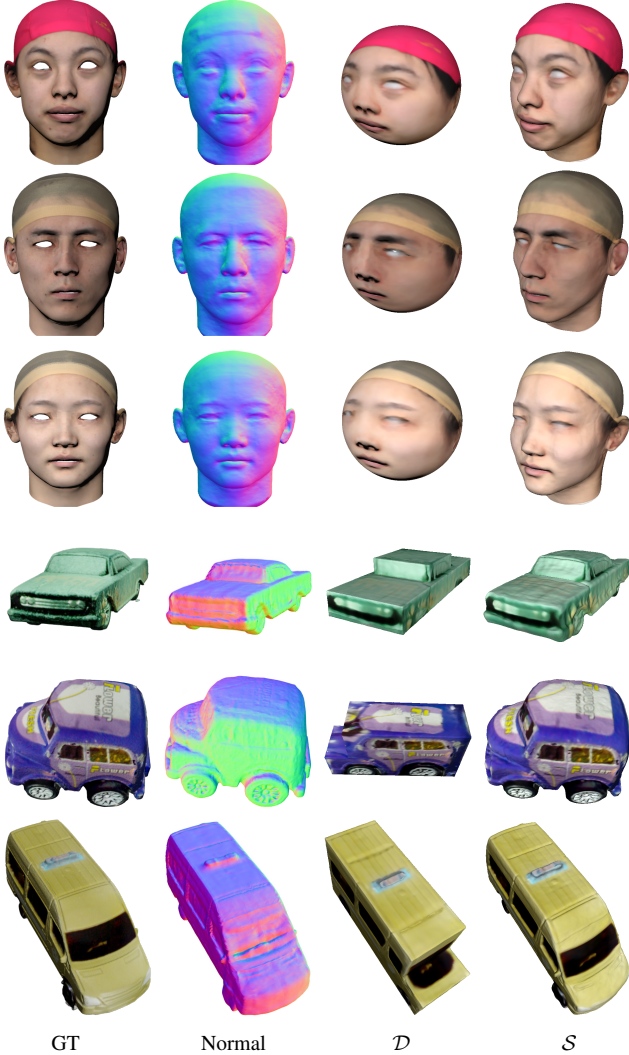


Figure 3. Parameterization results. Human heads are co-parameterized to a sphere owing to the clear geometric resemblance (top four rows). Given the diverse geometry of cars, each is parameterized to a polycube domain (bottom three rows). From left to right: the input image, the normal map of the reconstructed geometry \mathcal{S} , the parametric domain \mathcal{D} , and the reconstructed surface \mathcal{S} . See supplementary material for additional results.

3.1. Bi-directional deformation

The bi-directional deformation module serves as the pivotal component within our neural parameterization framework. As illustrated in Figure 2, this module consists of two sub-

networks: F_{def} , which is responsible for the forward mapping from the original model to the parameter domain, and $F_{\text{inv-def}}$, which establishes the inverse mapping.

Let \mathcal{S} be the 3D surface and \mathcal{D} be the parametric domain; both are represented by the zero level-set of neural signed distance fields. For an arbitrary point $\mathbf{p} \in \mathcal{S}$, the forward deformation $F_{\text{def}}(\mathbf{p}, \mathbf{z}_s)$ computes a displacement vector, mapping the point \mathbf{p} to a corresponding point $\mathbf{p}' \in \mathcal{D}$ in the parametric domain as follows:

$$\mathbf{p}' = \mathbf{p} + F_{\text{def}}(\mathbf{p}, \mathbf{z}_s). \quad (1)$$

Conversely, we employ $F_{\text{inv-def}}$ to map points inversely from the parametric domain \mathcal{D} back to the original shape \mathcal{S} :

$$\mathbf{p}'' = \mathbf{p}' + F_{\text{inv-def}}(\mathbf{p}', \mathbf{z}_s), \quad (2)$$

where the point \mathbf{p}'' is expected to be in close proximity to \mathbf{p} . To encourage the smoothness and stability of the deformations, we impose an L_2 loss on the magnitude of the displacement vectors:

$$\mathcal{L}_{\text{smooth}} = \|F_{\text{def}}(\mathbf{p}, \mathbf{z}_s)\|_2 + \|F_{\text{inv-def}}(\mathbf{p}', \mathbf{z}_s)\|_2. \quad (3)$$

This loss helps minimize abrupt and irregular deformations, leading to more coherent and gradual changes between \mathcal{S} and \mathcal{D} .

In training the networks F_{def} and $F_{\text{inv-def}}$, our objective is to achieve a bijective mapping between the 3D surface \mathcal{S} and the parametric domain \mathcal{D} . To achieve this goal, we adopt a cycle loss, which is similar to NeuTex [53]:

$$\mathcal{L}_{\text{cycle}} = \sum_{\mathbf{p} \in \mathcal{S}} \lambda(\mathbf{p}) \|\mathbf{p} - \mathbf{p}''\|_2, \quad (4)$$

where the weight λ characterizes the importance of sample \mathbf{p} to the loss. The reason that we do not consider all sample points equally is that a sample point may not be exactly on the zero level-set of the SDF. To tolerate such an inaccuracy, we define $\lambda(\mathbf{p}) = T(\mathbf{p})(1 - \exp(-\sigma(s)\delta(\mathbf{p})))$ as the color weight used in volume rendering [29]. Here, $T(\mathbf{p})$ is the transparency of sample \mathbf{p} in the viewing direction, δ is the length of the sample interval along the ray, and s is the signed distance value of the point \mathbf{p} . Clearly, when \mathbf{p} is away from the surface, the coefficient $\lambda(\mathbf{p})$ has few effects on this loss. We refer the readers to [29] for details about volume rendering and the computation of transparency T .

By explicitly minimizing the distance between \mathbf{p} and \mathbf{p}'' , the cycle loss effectively prevents scenarios where two distinct points $\mathbf{p}_1, \mathbf{p}_2 \in \mathcal{S}$ map to an identical point $\mathbf{p}' \in \mathcal{D}$. In such cases, the inverse deformation $F_{\text{inv-def}}$ would be unable to map the single point \mathbf{p}' back to the respective distinct points \mathbf{p}_1'' and \mathbf{p}_2'' .

Remark. It is worth mentioning that while our framework involves two SDFs - one for the 3D surface \mathcal{S} and the other for the parametric domain \mathcal{D} - our network design

only requires one of them. This is because one SDF can be derived from the other via either the forward or the backward deformation. To reduce the network complexity, we only adopt one geometry sub-network F_{sdf} , which is used to represent the parametric domain \mathcal{D} . Given a sphere, a cube, or a polycube, we pretrain the SDF sub-network to encode \mathcal{D} 's geometry. Leveraging the inherent smoothness of MLPs, the resulted SDF is smooth, aiding the computation of Laplacian.

3.2. Laplacian Regularization

Mitigating angle distortion is crucial in ensuring the quality of parameterization. One approach to reduce angle distortion involves minimizing the ratio of the two singular values of the Jacobian matrix associated with the parameterization [6]. However, considering the representation of the surface \mathcal{S} , the parametric domain \mathcal{D} , and the parameterization F_{def} as neural implicit functions in our approach, directly computing the Jacobian matrix is a non-trivial task. To circumvent this, we employ a Laplacian regularizer in our implementation to control angle distortion. Achieving the minimizer of the Laplacian of the map results in a harmonic map. For genus-0 surfaces, harmonic maps are also conformal, which preserves angles [13]. Although for surfaces of higher genus, a harmonic map is not necessarily conformal, it still serves an effective tool for reducing angle distortion [12]. Specifically, for a sample point $\mathbf{p} \in \mathcal{S}$ and its neighboring points $\mathbf{q}_j \in \mathcal{S}$, the forward deformation maps them to $\mathbf{p}' \in \mathcal{D}$ and $\mathbf{q}'_j \in \mathcal{D}$, respectively. We compute the Laplacian of the sample \mathbf{p} as follows:

$$\Delta(\mathbf{p}) = \sum_{j=1}^m \omega_j (\mathbf{p}' - \mathbf{q}'_j). \quad (5)$$

Here, the weights w_j are defined using the metric from the original surface \mathcal{S} as:

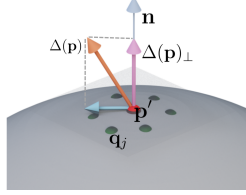
$$\omega_j = \exp(-\|\mathbf{p} - \mathbf{q}_j\|_2/l), \quad (6)$$

where l is the average distance from point \mathbf{p} to its neighboring points. Subsequently, the weights are normalized $\omega_j = \omega_j / \sum_{k=1}^m \omega_k$. Notice that $\Delta(\mathbf{p}) \in \mathbb{R}^3$ is a 3D vector, which may not necessarily lie on the tangent plane. Therefore, we define the normal component of the Laplacian as:

$$\Delta(\mathbf{p})_{\perp} = \langle \Delta(\mathbf{p}), \mathbf{n} \rangle \mathbf{n}, \quad (7)$$

where \mathbf{n} is the normal at \mathbf{p}' , and $\langle \cdot, \cdot \rangle$ represents the inner product. Summing the tangential components yields the Laplacian loss:

$$\mathcal{L}_{\text{Lap}} = \sum_{\mathbf{p} \in \mathcal{S}} \|\Delta(\mathbf{p}) - \Delta(\mathbf{p})_{\perp}\|_2. \quad (8)$$



In our implementation, we set $m = 6$ neighboring points for each sample \mathbf{p} .

3.3. Appearance Decomposition

Radiance represents the directional emission of color, illustrating how the appearance of an object varies in response to changes in the observational viewpoint [29]. Drawing inspiration from previous works [27, 62] and applying the assumptions of Lambertian and grayscale shading [4], we decompose the radiance field of the target surface into two components: a view-independent material field and a view-dependent shading field (see Figure 9 (b)). This decomposition allows for independent editing of material and shading. More precisely, for a sample point $\mathbf{p} \in \mathcal{S}$, we employ two sub-networks, F_{mat} and F_{shd} , to decompose the radiance $\mathbf{r} \in \mathbb{R}^3$ at point \mathbf{p} as follows:

$$\mathbf{r}(\mathbf{p}) = F_{\text{mat}}(\mathbf{p}', \mathbf{n}, \mathbf{z}_a) \cdot \exp(F_{\text{shd}}(\mathbf{p}', \mathbf{n}, \mathbf{v}, \mathbf{z}_a)), \quad (9)$$

where $\mathbf{p}' \in \mathcal{D}$ is the image of \mathbf{p} and \mathbf{n} is the unit normal of \mathbf{p} on the original surface. The material network F_{mat} takes the mapped point \mathbf{p}' , the surface normal \mathbf{n} , and the appearance latent code \mathbf{z}_a as input, generating the view-independent material field in response. The shading network F_{shd} , which is designed for computing the view-dependent shading field, takes an additional input: the viewpoint \mathbf{v} . To ensure the shading sub-network F_{shd} concentrates on **local** shading features, we employ an L_1 loss to the output of F_{shd} , encouraging sparsity,

$$\mathcal{L}_{\text{shd}} = \|F_{\text{shd}}(\mathbf{p}', \mathbf{n}, \mathbf{v}, \mathbf{z}_a)\|_1. \quad (10)$$

To compute the color, we need the signed distance values for the samples \mathbf{p} . As mentioned above, our network adopts only one SDF network F_{sdf} , which represents the geometry of the parametric domain \mathcal{D} . We use the forward deformation F_{def} to compute $s(\mathbf{p})$ as

$$s(\mathbf{p}) = F_{\text{sdf}}(\mathbf{p} + F_{\text{def}}(\mathbf{p}, \mathbf{z}_s)). \quad (11)$$

Then we employ the SDF-based volume rendering [61] to integrate the radiances along the ray to compute color $\mathbf{c}_{\text{pred}} = \sum_i \lambda_i \mathbf{r}_i$, where \mathbf{r}_i is the radiance of a sample point \mathbf{p}_i and λ_i is the same color weight as used in Equation (4).

3.4. Choice of Parametric Domains

An ideal parameterization should be conformal and area-preserving to avoid any signal distortion. For general objects, the overall parameterization to 2D domains, such as disks or squares, leads to large distortion. Thus, the standard 2D texture mapping is to cut the surface into several patches, each of which can be parameterized with low distortion. However, this multi-chart approach inevitably produces seams, and the process of creating a good overall

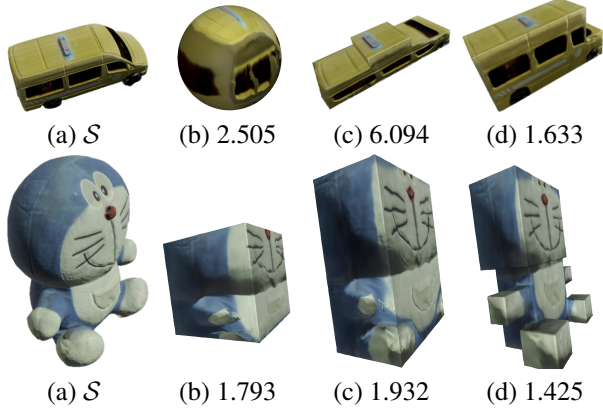


Figure 4. We offer the flexibility to choose from a range of parametric domains for managing area distortion. The closer the parametric domain \mathcal{D} ((b-d)) to the (a) 3D surface \mathcal{S} , the lower the area distortion $\mathcal{E}_{\text{area}}$ (shown below the objects, with a detailed definition provided in Section 4) in the parameterization.

mapping also requires one to define suitable boundaries of the charts in the 2D domain. Therefore, unlike NeP [27], we map the neural implicit surfaces to 3D parametric domains and provide the selection of an appropriate domain shape to reduce area distortion. In addition, we use the Laplacian regularizer to reduce angle distortion. Given the existence of infinite conformal maps [18], identifying those with minimal area distortion is highly desired. Area distortion is influenced by the similarity between the 3D surface and the parametric domain: the closer their alignment, the less the distortion. Thus, a simplistic, closely aligned parametric domain is ideal, balancing simplicity and alignment. Our algorithm accommodates various domains such as spheres, cubes, and polycubes, allowing flexibility in selection. It should be noted that our method supports more complex parametric domains, such as polyhedral complexes [59], thanks to the representation capability of the SDF sub-network. In our current implementation, we use spheres, cubes and polycubes, mainly because of their simplicity. Figure 4 illustrates the impact on the choice of parametric domain to the parameterization quality.

3.5. Training Losses

In contrast to NeP [27], which necessitate prior information such as tracked mesh and UV mapping for supervision, our method is capable of reconstructing 3D geometry and computing the corresponding texture map directly from multi-view images. This process is supervised by the image loss

$$\mathcal{L}_{\text{rgb}} = \|\mathbf{c}_{\text{gt}} - \mathbf{c}_{\text{pred}}\|_1, \quad (12)$$

where \mathbf{c}_{gt} and \mathbf{c}_{pred} are the ground-truth and predicted colors, respectively. To ensure the shape and appearance latent codes, \mathbf{z}_s and \mathbf{z}_a , conform to Gaussian distributions, we incorporate a regularization term, expressed as $\mathcal{L}_{\text{code}} =$

$\|\mathbf{z}_s\|_2 + \|\mathbf{z}_a\|_2$ [33]. Additionally, since both the 3D surface \mathcal{S} and the parametric domain \mathcal{D} are represented as signed distance fields, we employ the Eikonal loss [10, 60], defined as $\mathcal{L}_{\text{Eik}} = (\|\nabla s\|_2 - 1)^2$. Putting it all together, we define the total loss function as follows:

$$\begin{aligned} \mathcal{L} = & \mathcal{L}_{\text{rgb}} + \lambda_1 \mathcal{L}_{\text{Eik}} + \lambda_2 \mathcal{L}_{\text{cycle}} + \lambda_3 \mathcal{L}_{\text{smooth}} \\ & + \lambda_4 \mathcal{L}_{\text{Lap}} + \lambda_5 \mathcal{L}_{\text{shd}} + \lambda_6 \mathcal{L}_{\text{code}}. \end{aligned} \quad (13)$$

In our implementation, we empirically set the coefficients as $\lambda_1 = \lambda_2 = \lambda_5 = \lambda_6 = 0.01$ and $\lambda_3 = \lambda_4 = 0.001$.

4. Experiments

Datasets. For our experiments, we used a customized dataset named FS-Syn, derived from the Facescape dataset [58]. From Facescape, we selected 10 human head models and configured 30 fixed viewpoints and lighting conditions for each to obtain synthesized multi-view images. We also evaluated our method on several man-made objects from the DTU dataset [17] and the OmniObject dataset [52].

Training details and metric. All the sub-networks F_{def} , $F_{\text{inv-def}}$, F_{sdf} , F_{mat} , and F_{shd} are MLPs. See supplementary material for other detailed network hyperparameters. We trained our network using the Adam [19] optimizer. Once the parametric domain is chosen, we first trained F_{sdf} for 2,000 iterations to obtain the implicit neural representation of the parametric domain. Subsequently, we fixed F_{sdf} and trained other sub-networks for 2,000 epochs driven by the loss function as Equation (13). The quality of the polycube map is measured by the angle distortion and area distortion [3, 15] $\mathcal{E}_{\text{angle}}$, $\mathcal{E}_{\text{area}}$ as follows:

$$\mathcal{E}_{\text{angle}} = \frac{\cot \alpha |a|^2 + \cot \beta |b|^2 + \cot \gamma |c|^2}{4 \text{area}(\Delta_i)}, \quad (14)$$

$$\mathcal{E}_{\text{area}} = \frac{1}{2} \left(\frac{\text{area}(\Delta_i)}{\text{area}(\hat{\Delta}_i)} + \frac{\text{area}(\hat{\Delta}_i)}{\text{area}(\Delta_i)} \right), \quad (15)$$

where a, b, c represent the side lengths of the triangle Δ_i of the original surface. α, β, γ are angles of the corresponding triangle $\hat{\Delta}_i$ in parametric domain. In the case of conformal mapping, $\mathcal{E}_{\text{angle}}$ is equal to 1, and $\mathcal{E}_{\text{area}}$ is also equal to 1 for an isometric map.

Results. Our neural parameterization framework enables the construction of a bijective map between objects and multiple parametric domains such as spheres, cubes, and polycubes, as shown in Figure 3 and Figure 5. Additionally, our method supports co-parameterization of multiple objects and facilitates the transfer of material and shading between them. Our neural parameterization algorithm is fully compatible with existing neural rendering pipelines. Given multi-view images as input, we can reconstruct the 3D geometry and create the texture maps simultaneously.

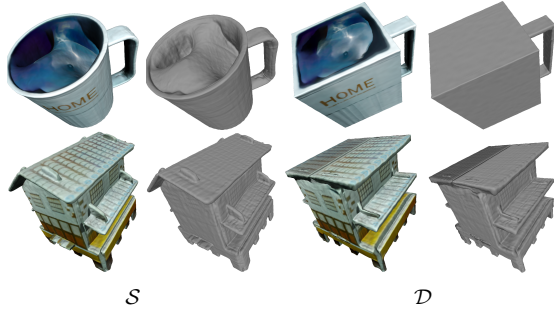


Figure 5. Parameterization results of objects with non-zero genus topology and complex shape.

As shown in Figure 3, we can obtain high-fidelity results without any prior information.

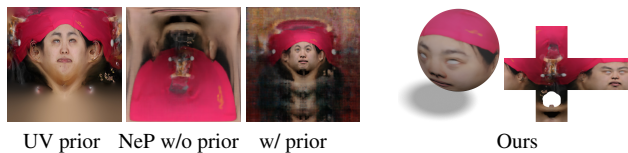


Figure 6. Parametrization results of NeP [27]

Compared with NeP [27], which is the latest neural surface editing work using neural parameterization, our method eliminates the need for prior information from UV mapping. Unlike our algorithm, NeP learns a map between surfaces and the UV plane. However, it heavily relies on an existing UV mapping as initialization, and yields rather poor texture mapping results without the UV mapping as prior (see Figure 6). Moreover, the results from NeP still exhibit significant distortions even with UV prior. Our method can effectively reduce angle distortion by minimizing Laplacian loss and reduce area distortion by choosing an appropriate parametric domain. As demonstrated in Figure 7, we calculate the angle distortion $\mathcal{E}_{\text{angle}}$ of parameterization as described in [3, 15]. We can observe that the Laplacian loss can effectively reduce angle distortion.

Radiance decomposition. In contrast to an entangled radiance field in NeRF [29] and VolSDF [61], we decompose the radiance into view-independent material and view-dependent shading according to Equation 9. We illustrate

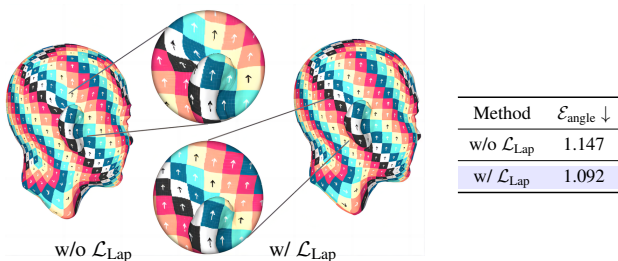


Figure 7. Ablation study. Utilization of the Laplacian loss has proven effective in reducing angle distortion ($\mathcal{E}_{\text{angle}}$), especially in regions with high curvature.

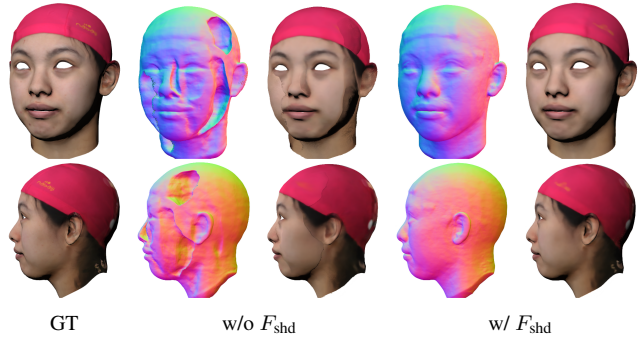


Figure 8. Ablation study. For scenes with significantly varying illumination, it is crucial to decompose view-dependent shading from the radiance field to further enable separate editing.

the decomposition results in Figure 9. We would like to emphasize that it is essential to decompose the radiance according to the view-dependent correlations for scenes with varying illumination. As shown in Figure 8 (down), it fails to reconstruct the 3D geometry when we remove the F_{shd} , and the visual quality drops subsequently.

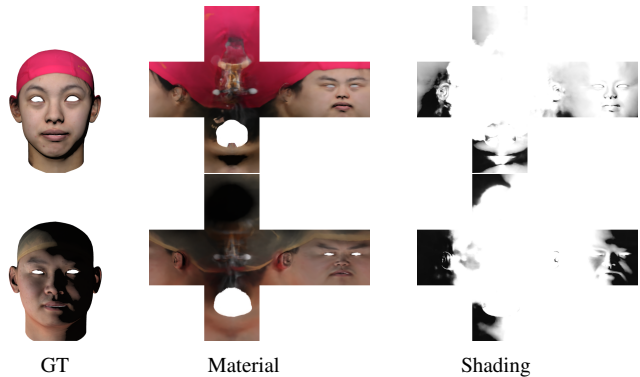


Figure 9. Radiance decomposition results.

Texture editing. Both NeuMesh [57] and NeP [27] can edit the object’s texture at a pixel level. We compare the editing and rendering results with NeuMesh and NeP, as shown in Figure 10. NeuMesh requires a mask of the editing region. It also re-trains the network after each edit, which is time-consuming and cannot guarantee the stability of the training results. Our method outperforms NeuMesh in terms of the visual quality. NeP, which is also neural parameterization-based method, requires a UV prior for initialization. It often yields poor parameterization results without such prior. Even with the UV prior, its parameterization results exhibit large distortion, making the edit in the 2D domain challenging. Our method is free of prior, and can yield parameterization with low distortion, thereby facilitating pixel-level editing and material transferring without network re-training.

Shading editing. We decompose the 3D radiance field into view-independent material and view-dependent shading.

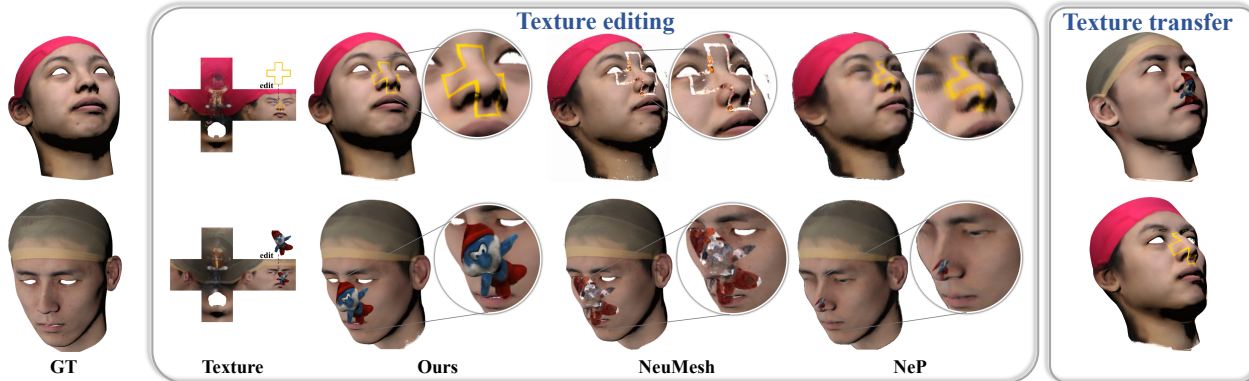


Figure 10. Representing the materials as textures defined in simple parametric domain enables easy editing. Also, our co-parameterization naturally supports texture transfer between different objects.

ing defined in the parametric domain. Taking advantage of this decomposition and the embedding into a simple domain, we can edit both the material and shading of the 3D surfaces in an intuitive manner. As illustrated in Figure 11, we modify the shading of one model by transferring the shading from another model under different lighting conditions, while keeping the material unchanged.

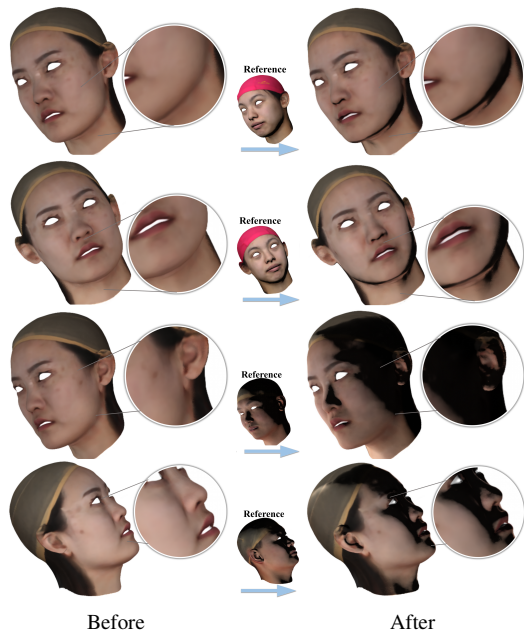


Figure 11. We transfer the decomposed shading from one model to another. See also the accompanying video.

5. Conclusion

We present a novel neural algorithm for parametrizing 3D surfaces represented by neural implicit functions to a user-defined parametric domain, such as a sphere, cube, or poly-cube. Utilizing bi-directional deformation, our method is

capable of learning a bijective mapping without relying on any prior knowledge, while controlling angle distortion through the usage of a Laplacian regularizer. Furthermore, our approach seamlessly integrates with the neural rendering pipeline, enabling the reconstruction of 3D objects from multi-view images and facilitating efficient volume rendering of modified textures and shadings — eliminating the necessity for network re-training. We demonstrated the efficacy of our method on human heads and man-made objects.

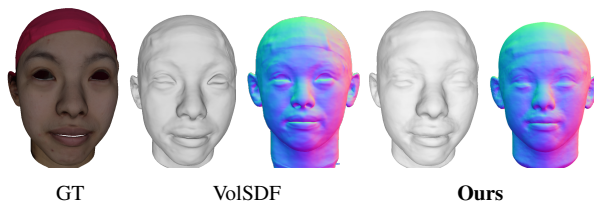


Figure 12. Geometry reconstruction results of VolSDF [61] and ours. Our method is capable of editing through parameterization, accompanied by an acceptable compromise in reconstruction quality.

Our method has a few limitations that require further improvement in the future. First, computational results on the FS-Syn dataset show that the reconstruction quality of our method is slightly worse than the standard SDF-based neural rendering algorithms, such as VolSDF [61] and NeuS [47]. For example, as illustrated in Fig. 12 and the right table, We report PSNR and CD compared with VolSDF [61] on Fs-Syn dataset [58]. This decline in visual quality arises from the incorporation of additional modules, such as bi-directional deformation and radiance decomposition, resulting in the cessation of updates to the SDF network within our neural parameterization pipeline. Therefore, computing a parameterization without compromising the reconstruction

| Method | PSNR | CD(10^{-3}) |
|--------|-------|-----------------|
| VolSDF | 31.15 | 3.270 |
| Ours | 30.87 | 3.423 |

quality is highly desired. Second, our radiance decomposition operates under the assumptions of Lambertian reflectance and grayscale shading, which might hinder its effectiveness when dealing with intricate materials or sophisticated shadings. Third, in our current implementation, we did not optimize the runtime performance. Therefore, training our model is time consuming, requiring 3 days for the 10 human heads of the FS-Syn dataset [58]. Incorporating recent advancements such as PermutoSDF [38] and Strivec [7] has the potential to significantly reduce the training and inference time.

References

- [1] Jan Bednarik, Shaifali Parashar, Erhan Gundogdu, Mathieu Salzmann, and Pascal Fua. Shape reconstruction by learning differentiable surface representations. In *Proceedings of the IEEE/CVF Conference on Computer Vision and Pattern Recognition*, pp. 4716–4725, 2020. 2
- [2] Henning Biermann, Ioana Martin, Fausto Bernardini, and Denis Zorin. Cut-and-paste editing of multiresolution surfaces. *ACM transactions on graphics (TOG)*, 21(3):312–321, 2002. 2
- [3] Patrick Degener, Jan Meseth, and Reinhard Klein. An adaptable surface parameterization method. *IMR*, 3: 201–213, 2003. 6, 7
- [4] Qingnan Fan, Jiaolong Yang, Gang Hua, Baoquan Chen, and David Wipf. Revisiting deep intrinsic image decompositions. In *Proceedings of the IEEE conference on computer vision and pattern recognition*, pp. 8944–8952, 2018. 5
- [5] Hui Fang and John C Hart. Textureshop: texture synthesis as a photograph editing tool. *ACM Transactions on Graphics (TOG)*, 23(3):354–359, 2004. 2
- [6] Michael S Floater and Kai Hormann. Surface parameterization: a tutorial and survey. *Advances in multiresolution for geometric modelling*, pp. 157–186, 2005. 2, 5
- [7] Quankai Gao, Qiangeng Xu, Hao Su, Ulrich Neumann, and Zexiang Xu. Strivec: Sparse tri-vector radiance fields. *arXiv preprint arXiv:2307.13226*, 2023. 9
- [8] Ismael García, Jiazhi Xia, Ying He, Shi-Qing Xin, and Gustavo Patow. Interactive applications for sketch-based editable polycube map. *IEEE Trans. Vis. Comput. Graph.*, 19(7):1158–1171, 2013. 2
- [9] Craig Gotsman, Xianfeng Gu, and Alla Sheffer. Fundamentals of spherical parameterization for 3d meshes. *ACM Trans. Graph.*, 22(3):358–363, 2003. 2
- [10] Amos Gropp, Lior Yariv, Niv Haim, Matan Atzmon, and Yaron Lipman. Implicit geometric regularization for learning shapes. In *International Conference on Machine Learning*, pp. 3789–3799. PMLR, 2020. 6
- [11] Thibault Groueix, Matthew Fisher, Vladimir G Kim, Bryan C Russell, and Mathieu Aubry. A papier-mâché approach to learning 3d surface generation. In *Proceedings of the IEEE conference on computer vision and pattern recognition*, pp. 216–224, 2018. 2
- [12] Xianfeng Gu and Shing-Tung Yau. Global conformal parameterization. In Leif Kobbelt, Peter Schröder, and Hugues Hoppe (eds.), *First Eurographics Symposium on Geometry Processing*, volume 43, pp. 127–137, 2003. 5
- [13] Xianfeng Gu, Yalin Wang, Tony F. Chan, Paul M. Thompson, and Shing-Tung Yau. Genus zero surface conformal mapping and its application to brain surface mapping. *IEEE Trans. Medical Imaging*, 23(8): 949–958, 2004. 5
- [14] Haoxiang Guo, Shilin Liu, Hao Pan, Yang Liu, Xin Tong, and Baining Guo. Complexgen: Cad reconstruction by b-rep chain complex generation. *ACM Transactions on Graphics (TOG)*, 41(4):1–18, 2022. 2
- [15] Ying He, Hongyu Wang, Chi-Wing Fu, and Hong Qin. A divide-and-conquer approach for automatic polycube map construction. *Computers & Graphics*, 33(3):369–380, 2009. 6, 7
- [16] Yi-Hua Huang, Yue He, Yu-Jie Yuan, Yu-Kun Lai, and Lin Gao. Stylizednerf: Consistent 3d scene stylization as stylized nerf via 2d-3d mutual learning. In *Computer Vision and Pattern Recognition (CVPR)*, 2022. 3, 1
- [17] Rasmus Jensen, Anders Dahl, George Vogiatzis, Engin Tola, and Henrik Aanæs. Large scale multi-view stereopsis evaluation. In *Proceedings of the IEEE conference on computer vision and pattern recognition*, pp. 406–413, 2014. 6, 1, 2
- [18] Miao Jin, Yalin Wang, Shing-Tung Yau, and Xianfeng Gu. Optimal global conformal surface parameterization. In *IEEE Vis 2004*, pp. 267–274, 2004. 6
- [19] Diederik P Kingma and Jimmy Ba. Adam: A method for stochastic optimization. *arXiv preprint arXiv:1412.6980*, 2014. 6
- [20] Zhengfei Kuang, Fujun Luan, Sai Bi, Zhixin Shu, Gordon Wetzstein, and Kalyan Sunkavalli. Palettenerf: Palette-based appearance editing of neural radiance fields. In *Proceedings of the IEEE/CVF Conference on Computer Vision and Pattern Recognition*, pp. 20691–20700, 2023. 1, 3
- [21] Manyi Li and Hao Zhang. D2im-net: Learning detail disentangled implicit fields from single images. In *Proceedings of the IEEE/CVF Conference on Computer Vision and Pattern Recognition*, pp. 10246–10255, 2021. 3

- [22] Zhaoshuo Li, Thomas Müller, Alex Evans, Russell H Taylor, Mathias Unberath, Ming-Yu Liu, and Chen-Hsuan Lin. Neuralangelo: High-fidelity neural surface reconstruction. In *Proceedings of the IEEE/CVF Conference on Computer Vision and Pattern Recognition*, pp. 8456–8465, 2023. [3](#)
- [23] Zhengqin Li, Jia Shi, Sai Bi, Rui Zhu, Kalyan Sunkavalli, Miloš Hašan, Zexiang Xu, Ravi Ramamoorthi, and Manmohan Chandraker. Physically-based editing of indoor scene lighting from a single image. In *European Conference on Computer Vision*, pp. 555–572. Springer, 2022. [3](#)
- [24] Connor Lin, Niloy Mitra, Gordon Wetzstein, Leonidas J Guibas, and Paul Guerrero. Neuform: Adaptive overfitting for neural shape editing. *Advances in Neural Information Processing Systems*, 35: 15217–15229, 2022. [3](#)
- [25] Steven Liu, Xiuming Zhang, Zhoutong Zhang, Richard Zhang, Jun-Yan Zhu, and Bryan Russell. Editing conditional radiance fields. In *Proceedings of the IEEE/CVF international conference on computer vision*, pp. 5773–5783, 2021. [1](#)
- [26] Weng Fei Low and Gim Hee Lee. Minimal neural atlas: Parameterizing complex surfaces with minimal charts and distortion. In *European Conference on Computer Vision*, pp. 465–481. Springer, 2022. [2](#)
- [27] Li Ma, Xiaoyu Li, Jing Liao, Xuan Wang, Qi Zhang, Jue Wang, and Pedro V Sander. Neural parameterization for dynamic human head editing. *ACM Transactions on Graphics (TOG)*, 41(6):1–15, 2022. [2](#), [3](#), [5](#), [6](#), [7](#), [1](#)
- [28] Lars Mescheder, Michael Oechsle, Michael Niemeyer, Sebastian Nowozin, and Andreas Geiger. Occupancy networks: Learning 3d reconstruction in function space. In *Proceedings of the IEEE/CVF conference on computer vision and pattern recognition*, pp. 4460–4470, 2019. [3](#)
- [29] Ben Mildenhall, Pratul P. Srinivasan, Matthew Tancik, Jonathan T. Barron, Ravi Ramamoorthi, and Ren Ng. Nerf: Representing scenes as neural radiance fields for view synthesis. In *ECCV*, 2020. [1](#), [4](#), [5](#), [7](#)
- [30] Thomas Müller, Alex Evans, Christoph Schied, and Alexander Keller. Instant neural graphics primitives with a multiresolution hash encoding. *ACM Transactions on Graphics (ToG)*, 41(4):1–15, 2022. [3](#)
- [31] Michael Niemeyer and Andreas Geiger. Giraffe: Representing scenes as compositional generative neural feature fields. In *Proc. IEEE Conf. on Computer Vision and Pattern Recognition (CVPR)*, 2021. [3](#)
- [32] Michael Oechsle, Songyou Peng, and Andreas Geiger. Unisurf: Unifying neural implicit surfaces and radiance fields for multi-view reconstruction. In *Proceedings of the IEEE/CVF International Conference on Computer Vision*, pp. 5589–5599, 2021. [1](#)
- [33] Jeong Joon Park, Peter Florence, Julian Straub, Richard Newcombe, and Steven Lovegrove. DeepSDF: Learning continuous signed distance functions for shape representation. In *Proceedings of the IEEE/CVF conference on computer vision and pattern recognition*, pp. 165–174, 2019. [3](#), [6](#)
- [34] Patrick Pérez, Michel Gangnet, and Andrew Blake. Poisson image editing. In *Seminal Graphics Papers: Pushing the Boundaries, Volume 2*, pp. 577–582. 2023. [3](#)
- [35] Emil Praun and Hugues Hoppe. Spherical parametrization and remeshing. *ACM transactions on graphics (TOG)*, 22(3):340–349, 2003. [2](#)
- [36] Charles R Qi, Hao Su, Matthias Nießner, Angela Dai, Mengyuan Yan, and Leonidas J Guibas. Volumetric and multi-view cnns for object classification on 3d data. In *Proceedings of the IEEE conference on computer vision and pattern recognition*, pp. 5648–5656, 2016. [3](#)
- [37] Charles R Qi, Hao Su, Kaichun Mo, and Leonidas J Guibas. Pointnet: Deep learning on point sets for 3d classification and segmentation. In *Proceedings of the IEEE conference on computer vision and pattern recognition*, pp. 652–660, 2017. [2](#)
- [38] Radu Alexandru Rosu and Sven Behnke. Permutosdf: Fast multi-view reconstruction with implicit surfaces using permutohedral lattices. In *Proceedings of the IEEE/CVF Conference on Computer Vision and Pattern Recognition*, pp. 8466–8475, 2023. [3](#), [9](#)
- [39] Zhixin Shu Sagnik Das, Ke Ma and Dimitris Samaras. Learning an isometric surface parameterization for texture unwrapping. In *European Conference of Computer Vision 2022, ECCV 2022, Tel Aviv, Israel, October 23-27, 2022*. Springer, 2022. [3](#)
- [40] Shunsuke Saito, Zeng Huang, Ryota Natsume, Shigeo Morishima, Angjoo Kanazawa, and Hao Li. Pifu: Pixel-aligned implicit function for high-resolution clothed human digitization. In *Proceedings of the IEEE/CVF international conference on computer vision*, pp. 2304–2314, 2019. [3](#)
- [41] Alla Sheffer, Emil Praun, Kenneth Rose, et al. Mesh parameterization methods and their applications. *Foundations and Trends® in Computer Graphics and Vision*, 2(2):105–171, 2007. [2](#)
- [42] Pratul P. Srinivasan, Boyang Deng, Xiuming Zhang, Matthew Tancik, Ben Mildenhall, and Jonathan T. Barron. Nerv: Neural reflectance and visibility fields for relighting and view synthesis. In *CVPR*, 2021. [3](#)
- [43] Qian Sun, Long Zhang, Minqi Zhang, Xiang Ying, Shi-Qing Xin, Jiazhi Xia, and Ying He. Texture brush:

- an interactive surface texturing interface. pp. 153–160, 2013. [2](#)
- [44] Marco Tarini, Kai Hormann, Paolo Cignoni, and Claudio Montani. Polycube-maps. *ACM transactions on graphics (TOG)*, 23(3):853–860, 2004. [2](#)
- [45] Kenji Tojo and Nobuyuki Umetani. Recolorable posterization of volumetric radiance fields using visibility-weighted palette extraction. In *Computer Graphics Forum*, volume 41, pp. 149–160. Wiley Online Library, 2022. [1](#), [3](#)
- [46] Nanyang Wang, Yinda Zhang, Zhuwen Li, Yanwei Fu, Wei Liu, and Yu-Gang Jiang. Pixel2mesh: Generating 3d mesh models from single rgb images. In *Proceedings of the European conference on computer vision (ECCV)*, pp. 52–67, 2018. [3](#)
- [47] Peng Wang, Lingjie Liu, Yuan Liu, Christian Theobalt, Taku Komura, and Wenping Wang. Neus: Learning neural implicit surfaces by volume rendering for multi-view reconstruction. *NeurIPS*, 2021. [1](#), [8](#)
- [48] Xiangyu Wang, Jingsen Zhu, Qi Ye, Yuchi Huo, Yunlong Ran, Zhihua Zhong, and Jiming Chen. Seal-3d: Interactive pixel-level editing for neural radiance fields, 2023. [1](#), [3](#)
- [49] Yifan Wang, Lukas Rahmann, and Olga Sorkine-Hornung. Geometry-consistent neural shape representation with implicit displacement fields. In *The Tenth International Conference on Learning Representations*. OpenReview, 2022. [3](#)
- [50] Yiqun Wang, Ivan Skorokhodov, and Peter Wonka. Hf-neus: Improved surface reconstruction using high-frequency details. *Advances in Neural Information Processing Systems*, 35:1966–1978, 2022. [3](#)
- [51] Francis Williams, Teseo Schneider, Claudio Silva, Denis Zorin, Joan Bruna, and Daniele Panozzo. Deep geometric prior for surface reconstruction. In *Proceedings of the IEEE/CVF conference on computer vision and pattern recognition*, pp. 10130–10139, 2019. [2](#)
- [52] Tong Wu, Jiarui Zhang, Xiao Fu, Yuxin Wang, Jiawei Ren, Liang Pan, Wayne Wu, Lei Yang, Jiaqi Wang, Chen Qian, Dahua Lin, and Ziwei Liu. Omniobject3d: Large-vocabulary 3d object dataset for realistic perception, reconstruction and generation. 2023. [6](#)
- [53] Fanbo Xiang, Zexiang Xu, Miloš Hašan, Yannick Hold-Geoffroy, Kalyan Sunkavalli, and Hao Su. NeuTex: Neural Texture Mapping for Volumetric Neural Rendering. In *The IEEE Conference on Computer Vision and Pattern Recognition (CVPR)*, 2021. [2](#), [3](#), [4](#), [1](#)
- [54] Baixin Xu, Jiarui Zhang, Kwan-Yee Lin, Chen Qian, and Ying He. Deformable model driven neural rendering for high-fidelity 3d reconstruction of human heads under low-view settings. In *Proceedings of the IEEE/CVF International Conference on Computer Vision*, 2023. [1](#), [3](#)
- [55] Tianhan Xu and Tatsuya Harada. Deforming radiance fields with cages. In *European Conference on Computer Vision*, pp. 159–175. Springer, 2022. [3](#)
- [56] Bangbang Yang, Yinda Zhang, Yinghao Xu, Yijin Li, Han Zhou, Hujun Bao, Guofeng Zhang, and Zhaopeng Cui. Learning object-compositional neural radiance field for editable scene rendering. In *International Conference on Computer Vision (ICCV)*, October 2021. [3](#)
- [57] Bangbang Yang, Chong Bao, Junyi Zeng, Hujun Bao, Yinda Zhang, Zhaopeng Cui, and Guofeng Zhang. Neumesh: Learning disentangled neural mesh-based implicit field for geometry and texture editing. In *European Conference on Computer Vision*, pp. 597–614. Springer, 2022. [3](#), [7](#), [1](#)
- [58] Haotian Yang, Hao Zhu, Yanru Wang, Mingkai Huang, Qiu Shen, Ruigang Yang, and Xun Cao. Facescape: a large-scale high quality 3d face dataset and detailed riggable 3d face prediction. In *Proceedings of the IEEE/CVF conference on computer vision and pattern recognition*, pp. 601–610, 2020. [6](#), [8](#), [9](#), [1](#)
- [59] Lei Yang, Yongqing Liang, Xin Li, Congyi Zhang, Guying Lin, Alla Sheffer, Scott Schaefer, John Keyser, and Wenping Wang. Neural parametric surfaces for shape modeling. *arXiv preprint arXiv:2309.09911*, 2023. [2](#), [6](#)
- [60] Lior Yariv, Yoni Kasten, Dror Moran, Meirav Galun, Matan Atzmon, Basri Ronen, and Yaron Lipman. Multiview neural surface reconstruction by disentangling geometry and appearance. *Advances in Neural Information Processing Systems*, 33, 2020. [6](#)
- [61] Lior Yariv, Jiatao Gu, Yoni Kasten, and Yaron Lipman. Volume rendering of neural implicit surfaces. *Advances in Neural Information Processing Systems*, 34:4805–4815, 2021. [1](#), [5](#), [7](#), [8](#)
- [62] Weicai Ye, Shuo Chen, Chong Bao, Hujun Bao, Marc Pollefeys, Zhaopeng Cui, and Guofeng Zhang. IntrinsicNeRF: Learning Intrinsic Neural Radiance Fields for Editable Novel View Synthesis. In *Proceedings of the IEEE/CVF International Conference on Computer Vision*, 2023. [3](#), [5](#)
- [63] Tarun Yenamandra, Ayush Tewari, Florian Bernard, Hans-Peter Seidel, Mohamed Elgharib, Daniel Cremers, and Christian Theobalt. i3dmm: Deep implicit 3d morphable model of human heads. In *Proceedings of the IEEE/CVF Conference on Computer Vision and Pattern Recognition*, pp. 12803–12813, 2021. [1](#), [3](#), [2](#)
- [64] Yu-Jie Yuan, Yang-Tian Sun, Yu-Kun Lai, Yuewen Ma, Rongfei Jia, and Lin Gao. Nerf-editing: geometry editing of neural radiance fields. In *Proceedings of the*

of the *IEEE/CVF Conference on Computer Vision and Pattern Recognition*, pp. 18353–18364, 2022. [3](#)

- [65] Yu-Jie Yuan, Yang-Tian Sun, Yu-Kun Lai, Yuewen Ma, Rongfei Jia, Leif Kobbelt, and Lin Gao. Interactive nerf geometry editing with shape priors. *IEEE Transactions on Pattern Analysis and Machine Intelligence*, 2023. [3](#)
- [66] Qijian Zhang, Junhui Hou, Yue Qian, Antoni B. Chan, Juyong Zhang, and Ying He. Reggeonet: Learning regular representations for large-scale 3d point clouds. *Int. J. Comput. Vis.*, 130(12):3100–3122, 2022. [2](#)
- [67] Qijian Zhang, Junhui Hou, Yue Qian, Yiming Zeng, Juyong Zhang, and Ying He. Flattening-net: Deep regular 2d representation for 3d point cloud analysis. *IEEE Trans. Pattern Anal. Mach. Intell.*, 45(8):9726–9742, 2023. [2](#)

Parameterization-driven Neural Implicit Surfaces Editing

Supplementary Material

A. Implementation Details

In our framework, the bi-deformation networks F_{def} and $F_{\text{inv-def}}$, the SDF network F_{sdf} , the texture network F_{mat} , and the appearance network F_{shd} are all multilayer perceptrons, consisting of 8, 8, 8, 4, and 4 layers, respectively. Each of these hidden layers has 256 neurons. The latent shape codes z_s and the appearance codes z_a are 128-dimensional. Within the neural rendering process, we set the frequency of position encoding for positions and viewpoints as 6 and 4, respectively. In each iteration, we randomly sample 1024 pixels from each input image for training. As for other parameter settings related to neural field reconstruction, we refer mainly to the work of VolSDF [61].

Baseline implementation details. For static settings, we remove the warp module in the NeP [27]. Then we train NeP under two settings, one is under UV ground truth as supervision and the other is not (see Figure 13). The parameter configurations for other settings can be found in [27].

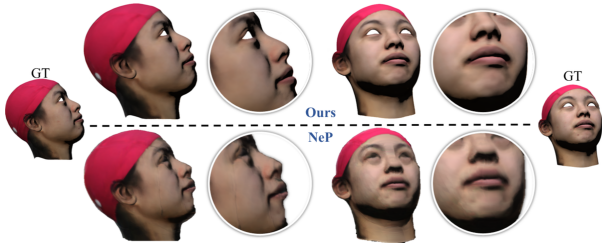


Figure 13. We compare the rendering results with NeP without prior information from UV mapping.

FS-Syn dataset preparation. We derived a customized dataset from Facescape [58], as shown in Figure 14. We randomly chose 10 human heads with neutral expressions from uniformly topologized models in the FaceScape dataset. Subsequently, we illuminated the human head model by moving both the light source and the camera, generating diverse lighting effects. Following this, we captured 30 images from different angles around the human head, each accompanied by its corresponding camera parameters.

B. Additional Results

We also tested our method on the DTU dataset [17] as shown in Figure 15(a). Moreover, our parameterization

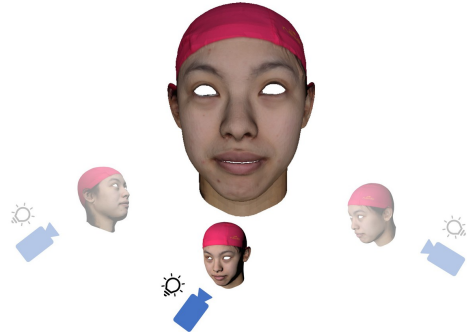


Figure 14. We create the FS-Syn dataset from the FaceScape dataset. We illuminated the human head by moving both the light source and the camera, creating varying lighting effects.

framework can be used to seamlessly stitch segmented texture maps together, as shown in Figure 15(b). In addition to texture and shading, our framework also can edit geometric details on original models based on parameterization results and the assigned displacement map, as illustrated in Figure 15(c).

C. Geometry Editing via Modifying the Parametric Domain \mathcal{D}

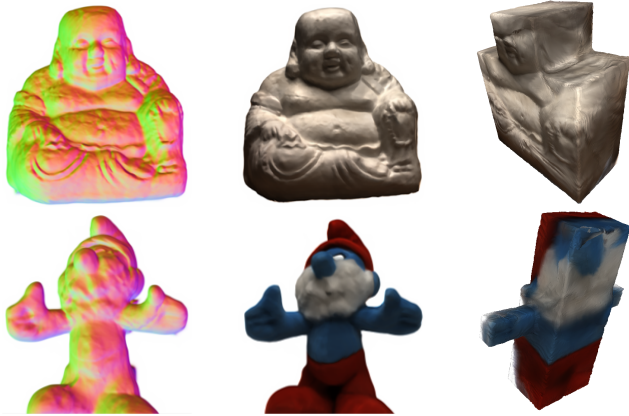
In addition to the 2D displacement map, we also provide a geometry-editing method (See Figure 16) based on the parametric domain. As shown in Figure 17, we remove the handle of the cup in the parametric domain, and then we render the cup model in volume rendering without any training again.

| Method | Level | Retraining | 3D input |
|-------------------|--------------|------------|----------|
| EditNeRF [25] | Object | Y | N |
| StylizedNeRF [16] | Scene | N | N |
| i3DMM [63] | Object | N | Y |
| NeuMesh [57] | Pixel | Y | N |
| Seal3D [48] | Pixel | Y | N |
| NeuTex [53] | Pixel | N | Y |
| NeP [27] | Pixel | N | Y |
| Ours | Pixel+Object | N | N |

Table 1. Qualitative comparison with other neural texture editing methods.

D. Qualitative Comparison

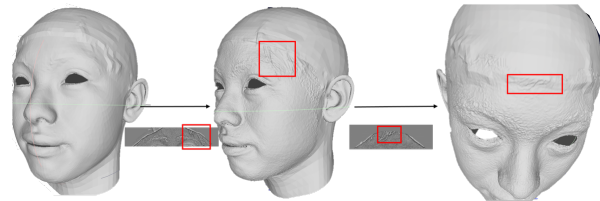
We summarize some parametrization methods (refer to Table 2) and some neural editing methods (refer to Table 3) to



(a)



(b)



(c)



(d)

Figure 15. Additional results: (a) Visualization of normal maps, neural rendering results, and parametric domain on models from the DTU dataset [17]. (b) Textures. The textures associated with the original meshes (middle) are discontinuous and exhibit significant distortion, making them less suitable for editing purposes. In contrast, the textures resulting from our parameterization (right) are globally continuous and exhibit minimal distortions. (c) Geometric detail editing. (d) Source geometry, target appearance, and texture transfer results. Durian and Apple undergo joint training as they belong to the same category.

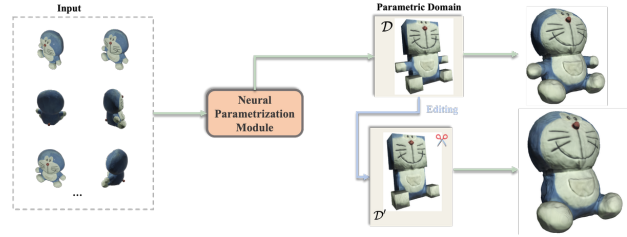


Figure 16. Pipeline of geometry editing on the parametric domain. We replace the original parametric domain with a modified one and immediately render the edited objects.



Figure 17. Editing the geometry of the parametric domain \mathcal{D} naturally induces a modified neural implicit surface. We edit the geometry of the cup by removing and deforming the handle in \mathcal{D} . The top row shows the original parametric domain \mathcal{D} and two modified domains. The bottom row shows the neural implicit surface \mathcal{S} corresponded to each parametric domain.

illustrate the effectiveness and superiority of our approach. As shown in Table 1, we categorize these texture editing methods with other editing methods into three groups: scene-level, object-level, and pixel-level editing. Scene-level editing methods focus on the entire appearance of a scene including lighting and material. Object-level editing methods employ distinct part-based latent codes to manipulate different attributes of a scene, such as hairstyles in i3DMM [63]. Pixel-level editing, on the other hand, offers a fine-grained editing result by taking into account precise user guidance.

| Method | Representation | Prior | Rendering | Regularization | Texture | Domain |
|-------------|----------------|--------------|-----------|----------------|--------------|-------------------|
| NeuTex [53] | Density | Init. UV-inv | V.R. | NA | Entangled | Sphere |
| ISO-UV [39] | SDF | Init. UV | D.R. | Jacobian | Entangled | \mathbb{R}^2 |
| NeP [27] | Density | Mesh & UV | V.R. | Angle | Disentangled | \mathbb{R}^2 |
| Ours | SDF | None | V.R. | Laplace | Disentangled | Sphere & polycube |

Table 2. Qualitative comparison with other neural parameterization methods. V.R. and D.R. stand for volume rendering and differentiable rendering, respectively.

| Method | Proxy | Deformation | Removal | Texture | Retraining | Category |
|-----------------------|-------------------|-------------|---------|---------|------------|----------|
| NeRF-Editing [64, 65] | Mesh | Y | N | N | N | N |
| NeuMesh [57] | Mesh | Y | N | Y | Y | N |
| DRFC [55] | Cage | Y | N | N | N | N |
| Ours | Parametric domain | Y | Y | Y | N | Y |

Table 3. Qualitative comparison with other methods for editing the geometry of neural radiance fields. While all these methods exhibit deformation capabilities, they encounter challenges of removing specific parts, such as a cup’s handle, as illustrated in Figure 17. By editing the parametric domain \mathcal{D} , we can immediately obtain the deformed neural implicit surfaces through inference on the modified domain \mathcal{D}' . Our method is trained on a specific category of objects, such as human heads and fruits. This specialized training enables our approach to transfer textures and geometries among objects in the same category.